Contrib. Plasma Phys. **41** (2001) 2-3, 275-278

Conductivity of Nonideal Zinc and Carbon Plasmas - Experiments and Theoretical Results

J. Haun[a], S. Kosse[b], H.-J. Kunze[a], M. Schlanges[b], R. Redmer[c]

[a]Institut für Experimentalphysik V, Ruhr-Universität Bochum, 44780 Bochum, Germany
[b]Institut für Physik, Ernst-Moritz-Arndt-Universität Greifswald, Domstr. 10a, 17489 Greifswald, Germany
[c]Fachbereich Physik, Universität Rostock, 18051 Rostock, Germany
e-mail:Jens.Haun@ep5.ruhr-uni-bochum.de

Abstract

In recent years it has become possible to produce and analyze dense, strongly coupled plasmas. In particular it was possible to determine transport properties.

In this contribution we report on measurements of the electrical conductivity of nonideal zinc and carbon plasmas, which are produced by evaporating a wire placed in a capillary (exploding wire) within some hundred nanoseconds. The particle density is in the range of 10^{22} cm^{-3}. The plasma temperature, which is obtained by fitting a Planck function to the measured spectrum, is between 8000 and 20000 K.

We compare the measured electrical conductivies with theoretical results using quantum kinetic theory for partially ionized plasmas. Here, the transport cross sections are calculated in T-matrix approximation and the plasma composition of the nonideal plasma is determined by the solution of coupled mass action laws.

1 Introduction

In the last decades there were several attempts to understand the physics of the electrical conductivity of strongly coupled metal plasmas. Today we can compare the latest measurements of carbon and zinc with the results of quantum kinetic theory for partially ionized plasmas.

We produce the nonideal plasmas at near-solid-state densities and temperatures lower than 20000 K by fast vaporisation of wires (exploding wire). This works very well for metals which have a high electrical conductivity. For the half metal carbon we had to develop a preheating system [1].

Nonideal plasmas are characterized by the coupling parameter Γ. It is defined as the ratio of the mean potential energy to mean kinetic energy: $\Gamma = (Z^2e^2)/(4\pi\epsilon_0 kTd_i)$, with $d_i = (3/4\pi n_i)^{(1/3)}$. It is given by the ion temperature T and the ion density n_i. Relating to the following measurements, we set $Z = 1$. The coupling parameter in our carbon plasma is in the range of $1 \leq \Gamma \leq 8$.

2 Experimental setup

The wire is surrounded by a glass capillary to achieve a longer confinement time of the exploding plasma, figure 1. Two capacitors connected in parallel, totaling 3.86 μF are charged to at least 20 kV to ensure vaporization of the wire. They are discharged by closing a low-inductive pressurized spark gap switch. A total inductance of only 154 nH makes sure that the current can rise rapidly. A Rogowski coil surrounds one

electrode to measure the time derivative of the current. The voltage is measured with two resistive voltage dividers. The emitted light is observed with two different spectrometers and an OMA system (Optical Multichannel System). A Planck curve is fitted to the measured spectrum to determine the temperature of the optically thick plasma. We assume the plasma is in LTE (Local Thermodynamic Equilibrium). The time depending radius of the plasma is recorded by an ICCD (Intensified Charge Coupled Device) camera and a streak camera.

The resistivity of carbon is high at room temperature and decreases with growing temperature. To ensure a good energy input and a homogeneous plasma a preheating system is used [1].

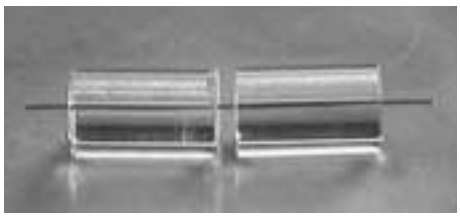

Fig. 1: Wire with surrounding capillary; here the capillary is cut in two pieces to use the possibility to view the plasma directly. Length: 24 mm, diameter of wire: 125 μm (zinc), 273 μm (carbon)

The voltage measured with the two voltage dividers consists of a resistive and an inductive component $U = IR + d/dt(LI)$. At the beginning of the discharge, the inductive component becomes important. Later the resistive component dominates. Since the change in inductance due to phase transitions is negligibly small, solving for the plasma conductivity σ yields

$$\sigma = \frac{l}{RA} = \frac{I}{U - L_D\dot{I}} \frac{l}{\pi r^2}. \tag{1}$$

3 Data analysis and behaviour of the discharge

Figure 2 shows two streak pictures. The white line at the very left part of the pictures is produced by a ruby laser. It is used to make a time calibration of the streak photos. Carbon and zinc behave quite different: The carbon plasma reaches the inner wall after 300 ns. Then the radius is constant for about 500 ns. The temperature is changing during this time continuously. Therefore the conductivity can be measured at one density for different temperatures.

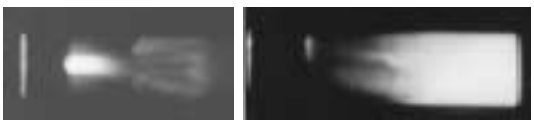

Fig. 2: Some examples of the streak pictures. Left: streak picture of carbon plasma, right: streak picture of zinc.

With zinc the current decreases when the plasma is being produced and has reached the inner part of the capillary. In the streak pictures the plasma is dark. It makes sense to measure the conductivity only during the very short time interval when the plasma has reached the inner part of the capillary. Therefore the conductivity is obtained only for one density and nearly one temperature. In the future the density will be changed by using different capillaries with different inner diameters.

4 Quantum kinetic approach to the electrical conductivity

Starting from the Boltzmann equation (expansion to Sonine polynomials and small deviation from equilibrium), we derived an expression for the electrical conductivity

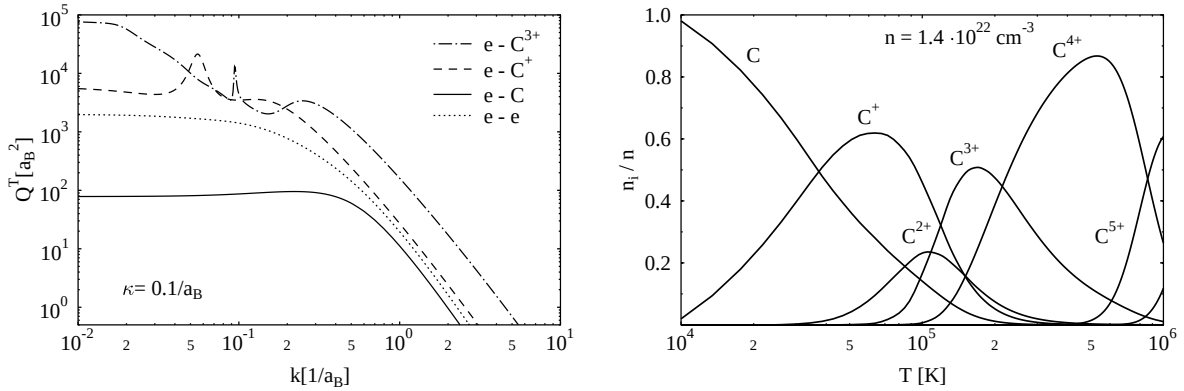

Fig. 3: Left: transport cross sections, κ is the inverse Debye length ($\kappa^2 = 2\mathrm{e}^2 n_e^*/(\epsilon_0 k_B T)$); Right: plasma composition for a carbon plasma.

for a partially ionized plasma [2]

$$\sigma_{(n)} = \frac{3\sqrt{\pi}}{8} \frac{\mathrm{e}^2 n_e^*}{\sqrt{2 m_e k_B T}} \frac{\begin{vmatrix} I^{11} & \cdots & I^{n1} \\ \vdots & & \vdots \\ I^{1n} & \cdots & I^{nn} \end{vmatrix}}{\begin{vmatrix} I^{00} & \cdots & I^{n0} \\ \vdots & & \vdots \\ I^{0n} & \cdots & I^{nn} \end{vmatrix}} \tag{2}$$

with the collision terms $I^{lm} = I_{ee}^{lm} + I_{ei}^{lm} + I_{eA}^{lm}$ and n being the order of approximation in the Sonine polynomial expansion. The electron–ion collision term has the form

$$I_{ei}^{00} = \frac{n_i}{2 m_e k_B T} \int_0^\infty \mathrm{d}p \, Q_{ei}^T(p) \, p^5 \exp\left(-\frac{p^2}{2 m_e k_B T} \right).$$

One can see that two main inputs determine the electrical conductivity, the plasma composition n_i and the transport cross section Q_{ei}^T.

The transport cross sections are determined by a phase shift analysis in T–matrix approximation (see e.g. [3, 4]). With the statically screened Coulomb potential for electron–ion and electron–electron interaction and the polarization potential for the electron–atom interaction, we obtain the transport cross sections shown in figure 3 (left).

To calculate the plasma composition, we consider the simple ionization processes $M^{(Z-1)+} \rightleftharpoons M^{(Z)+} + e$ (Z is the ionization stage with the ionization energy E_{ion}^Z). We arrive at a system of coupled mass action laws

$$n_{Z-1} = \frac{g_{Z-1}}{g_Z} n_Z \exp[\beta(E_{ion}^Z + \mu_e^{id} + \mu_e^{cor} + \mu_Z^{cor} - \mu_{Z-1}^{cor})]. \tag{3}$$

Here, n_a is the density, μ_a the chemical potential and g_a the statistical weight of the species a (electron, atom, ions), respectively. The correlation part of the chemical potential μ^{cor} is determined from a Padé–approximation [5]. Solving (3), we obtain the plasma composition shown in figure 3 (right) for a carbon plasma.

5 The conductivity results and comparison with theory

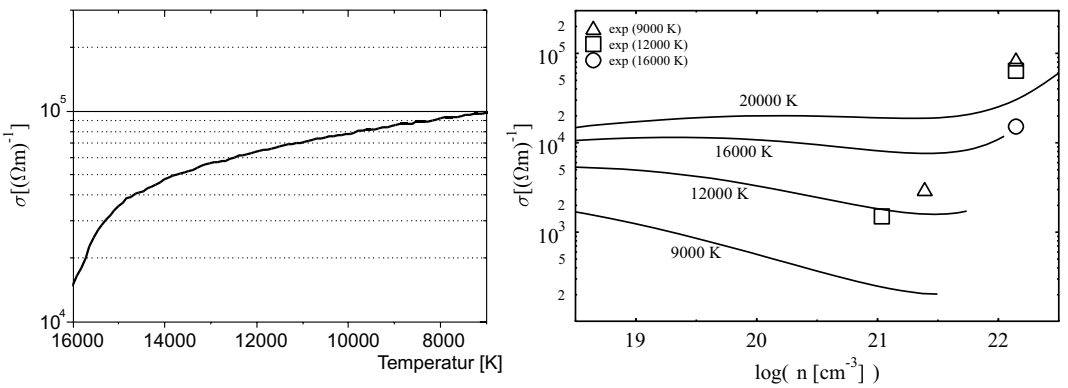

Fig. 4: Conductivity of carbon: left: $\rho = \text{const} = 0.28$ g cm$^{-3} \Longleftrightarrow n = 1.4 \times 10^{22}$ cm^{-3}; right: comparison with theory.

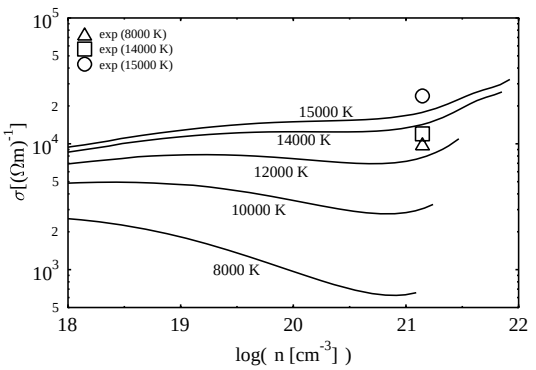

Fig. 5: Conductivity of zinc in comparison to the calculations.

The results for the conductivity of carbon are shown in figure 4. In the left picture the conductivity is measured as a function of the temperature at one density. In the right picture the measurements are compared with the calculations using eq. (2). Some data from earlier measurements are also considered in this graph [1]. Figure 5 shows the results for zinc.

For higher temperatures (T $>$ 12000 K), the experimental data are in good agreement with our theoretical results. For the low temperatures, we assume that the pressure ionization starts in the measured density region. Our simple mass action law (3) cannot describe the pressure ionization in the given parameter region correctly. Therefore, an important point for comparison with experimental data for low temperatures is the improved calculation of the plasma composition.

References

[1] J. Haun, Diplomarbeit (1997), J. Haun, H.-J. Kunze, Contrib.Plasma Phys. **39** (1999) 169.
[2] M. Schlanges, D. Kremp, H. Keuer, Ann. Phys. **41** (1984) 54.
[3] Ch.J. Joachain: Quantum Collision Theory (North–Holland, Amsterdam 1983).
[4] D.O. Gericke, S. Kosse, M. Schlanges, M. Bonitz, Phys. Rev. B **59** (1999) 10639.
[5] A. Förster, Doktorarbeit, Berlin 1991, W. Ebeling, A. Förster, V.E. Fortov, V.K. Gryaznov, A.Ya. Polishchuk: Thermophysical Properties of Hot Dense Plasmas (Teubner Verlagsgesellschaft, Stuttgart, Leipzig 1991) p. 39.

Received 24 October 2000, in final form 10 November 2000